An Overview of Network Bifurcations in the Functionalized Cahn-Hilliard Free Energy

Noa Kraitzman* & Keith Promislow†

October 5, 2014

Abstract

The functionalized Cahn-Hilliard (FCH) free energy models interfacial energy in amphiphilic phase-separated mixtures. Its minimizers and quasi-minimizers encompass rich classes of network morphologies with detailed inner layers incorporating bilayers, pore, pearled pore, and micelle type structures. We present an overview of the stability of the network morphologies as well as the competitive evolution of bilayer and pore morphologies under a gradient flow in 3 space-dimensions.

Key words: Functionalized Cahn Hilliard, Meander, Pearling, Strong Functionalization
AMS (MOS) subject classifications: 34E10, 35B35, 35PL15

1 Amphiphilic Materials

Traditionally, an amphiphilic molecule is one which finds its energetically favorable interaction at the interface of two disparate fluids, such as soap in oily water. Indeed, early studies of amphiphilic materials concerned emulsions formed from two immiscible fluids combined with an amphiphilic surfactant. Lipids, formed of a hydrophilic head group and a hydrophobic tail also belong to the class of amphiphilic molecules. More recently, developments in synthetic chemistry, such as atom transfer radical polymerization, have simplified the process of attaching charge groups to polymers, greatly expanding the possible classes of amphiphilic polymers that can be readily synthesized, see [Matyjaszewski (2012)] and [Charleux et al (2012)]. Amphiphilic blends typically phase separate, however the propensity of the amphiphilic molecules to form monolayers leads to an energetic preference for thin interfaces. As a result the interfaces are often co-dimension one bilayers, or co-dimension two pore structures – morphologies that are often referred to collectively as networks. And these networks have significant value: they self-assemble at the nano-scale, yielding huge densities of solvent-accessible surface area and are often charge-lined, which renders them effective as selective ionic conductors. Due to these traits, amphiphilic materials have found use in many types of energy conversion devices, forming the ionomer membranes in fuel cells, the photo-active collecting matrix in bulk-heterojunction solar cells, and the separator membrane in Lithium ion batteries.

The casting of blends of amphiphilic mixtures and di-block polymers presents a rich array of distinct morphologies, however control of the end-state morphology is experimentally challenging due to the delicate roles played by solvent type, salt concentration and counter-ion type, di-block composition and polydispersity, temperature, and pH. It has been shown, [Discher & Eisenberg (2002)], that changing the concentration of water in a water-dioxane solvent blend induces bifurcations in amphiphilic di-blocks yielding micelle, micelle-pore, pore, pore-vesicle, and vesicle network morphologies. Similar

*Department of Mathematics, Michigan State University, kraitzm1@msu.edu
†Department of Mathematics, Michigan State University, kpromisl@math.msu.edu

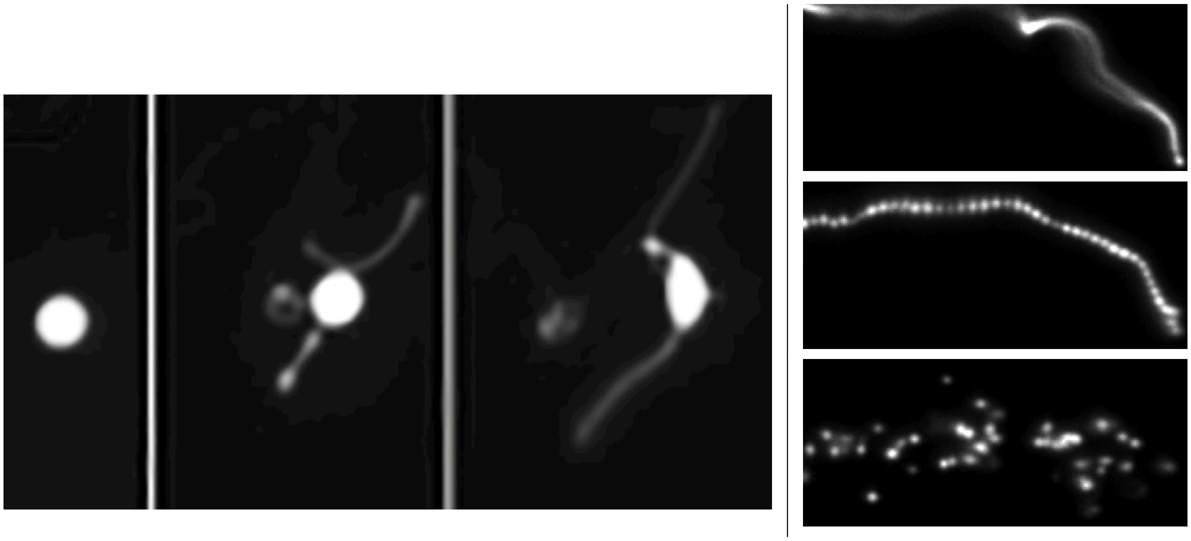

Figure 1.1: Szostak's mechanism for division of primitive cell membrane: (left) raising the background concentration of lipids induces the vesicle to grow worm-like (co-dimension two) protusions over a 74 nano-second time period [Budin & Szostak (2011)], (right) changing the density of charged groups on the surface via a photochemically induced redox reaction incites the pore to pearl and break into micelles [Zhu et al (2012)]. Reprint permission grunted by Proceedings of National Academy of Science.

Szostak

bifurcation were obtained in PEO-PB amphiphilic di-blocks by changing the density of charge groups in the hydrophilic portion, [Jain & Bates (2004)], or by varying the length of the hydrophobic portion of the di- block, [Ratcliffe et al (2013)]. Morphological reconfigurations can also be achieved through varying temperature, [Zare et al (2012)] and [Gomez et al (2005)], and concentrations of counter-ions [Zhulina & Borisov (2012)].

We pay particular attention to the experimental investigation in [Budin & Szostak (2011)] and [Zhu et al (2012)] of the division of primitive lipid membranes, for which a particularly simple method was devised to induce the bilayer to micelle bifurcations discussed above. Szostak's group formed a suspension of spherical vesicles of 10% phospholipid and found that increasing the concentration of free oleo-lipids dispersed in the bulk solvent induced a fingering instability in spherical phospholipid vesicles, depicted in the three horizontally arranged panels on the left side of Figure 1.1. The end state consisted of long, co-dimension two pore morphologies. In a subsequent experiment, the charge density of cylindrical pores was suddenly increased through a photo-oxidation process; the jump in charge density induced a pearling bifurcation causing the pore structures to break into individual micelles, as depicted in the three vertically arranged panels on the right side of Figure 1.1. The goal of this overview is present an analysis of related bifurcations within the context of the Functionalized Cahn-Hilliard free energy.

2 The Functionalized Cahn-Hilliard Free Energy

The Cahn-Hilliard free energy, [Cahn & Hilliard (1958)], describes the spinodal decomposition of a binary mixture. For a fixed domain, $\Omega \subset \mathbf{R}^3$, a phase function $u \in H^1(\Omega)$ describes the volume fraction of one component of the binary mixture, and the free energy is modeled a function of the density u weakly perturbed by the spatially isotropic gradients

$$\mathcal{E}(u) = \int_\Omega f(u, \varepsilon^2|\nabla u|^2, \varepsilon^2\Delta u)\, dx. \tag{2.1}$$

Expanding the free energy in orders of ε and truncating at $O(\varepsilon^4)$, yields an expression of the form

$$\mathcal{E}(u) = \int_\Omega f(u,0,0) + \varepsilon^2 A(u)|\nabla u|^2 + \varepsilon^2 B(u)\Delta u \, dx. \tag{2.2}$$

To obtain a generic normal form for the free energy, Cahn and Hilliard integrated by parts on the $B(u)$ term, set the resulting coefficient of $|\nabla u|^2$ to $\frac{1}{2}$, and renamed the potential $f(u,0,0)$ to $W(u)$. The result is the Cahn-Hilliard free energy

$$\mathcal{E}(u) = \int_\Omega \frac{\varepsilon^2}{2}|\nabla u|^2 + W(u)\, dx. \tag{2.3}$$

The corresponding H^{-1} gradient flow, the Cahn-Hilliard equation, takes the form

$$u_t = \Delta \frac{\delta \mathcal{E}}{\delta u} = \Delta(-\varepsilon^2 \Delta u + W'(u)). \tag{2.4}$$ e:CH-H1

Subject to traceless boundary conditions the Cahn-Hilliard equation preserves the total mass

$$\frac{d}{dt}\int_\Omega u(x,t)\, dx = 0, \tag{2.5}$$

and dissipates the Cahn-Hilliard free energy

$$\frac{d}{dt}\mathcal{E}(u) = \left\langle u_t, \frac{\delta \mathcal{E}}{\delta u}\right\rangle_{L^2} = -\left\| \nabla \frac{\delta \mathcal{E}}{\delta u}\right\|_{L^2}^2 \leq 0. \tag{2.6}$$

To model amphiphilic mixtures, such as emulsions formed by adding a minority fraction of an oil and soap mixture to water, [Teubner & Strey (1987)] and [Gompper & Schick (1990)] were motivated by small-angle X-ray scattering (SAXS) data to include a higher-order term in the usual Cahn-Hilliard expansion,

$$\mathcal{F}(u) := \int_\Omega f(u,0,0) + \varepsilon^2 A(u)|\nabla u|^2 + \varepsilon^2 B(u)\Delta u + \overbrace{C(u)}^{\geq 0}(\varepsilon^2 \Delta u)^2\, dx. \tag{2.7}$$

The full form of this system supports too many possible regimes to permit a systematic study. It is important to find the simplest mathematical framework that supports the network morphologies typical of amphiphilic mixtures; we need new normal form. With this goal we first shift all the differential terms to powers of Laplacians; specifically, letting $\overline{A}$ denote the primitive of A, we replace $A(u)\nabla u$ with $\nabla \overline{A}(u)$ and integrate by parts on the term $\nabla \overline{A} \cdot \nabla u$ to obtain

$$\mathcal{F}(u) = \int_\Omega f(u,0,0) + (B(u) - \overline{A}(u))\varepsilon^2 \Delta u + C(u)(\varepsilon^2 \Delta u)^2\, dx. \tag{2.8}$$

The energy density is a quadratic polynomial in $\varepsilon^2 \Delta u$, which suggests that we complete the square

$$\mathcal{F}(u) = \int_\Omega C(u)\left(\varepsilon^2 \Delta u - \frac{\overline{A} - B}{2C}\right)^2 + f(u,0,0) - \frac{(\overline{A} - B)^2}{4C(u)}\, dx. \tag{2.9}$$

For simplicity we replace $C(u)$ with $\frac{1}{2}$, and relabel the potential within and outside the squared term by $W'(u)$ and $P(u)$, respectively. The key point is that the first term is the square of the variational derivative of a Cahn-Hilliard type free energy, consequently the case $P \equiv 0$, when the energy is a perfect square, has the special property that its global minimizers are precisely the *critical points* of the corresponding Cahn-Hilliard energy. Indeed, a variant of this case was proposed as a target for

$\Gamma-$convergence analysis by De Giorgi, see [Roger & Schatzle (2006)]. The normal form of the network is obtained by unfolding the perfect square via a scaled perturbation

$$\mathcal{F}(u) = \int_\Omega \frac{1}{2}\left(\varepsilon^2 \Delta u - W'(u)\right)^2 + \delta P(u)\, dx, \tag{2.10}$$

where $\delta \ll 1$. The function $W(u)$ is assumed to be a double-well potential with two minima at $u = b_\pm$ whose unequal depths are normalized so that $W(b_-) = 0 > W(b_+)$. Typically $b_- = 0$, however it is helpful to give this value a specific name. Thus $u = b_-$ is associated to a bulk solvent phase, while the size of $u - b_- > 0$ is proportional to the density of the amphiphlic phase. The parameter $\varepsilon \ll 1$ determines interfacial width and corresponds to the ratio of the typical length of an amphiphilic molecule to the domain size.

The Functionalized Cahn-Hilliard free energy is a class of two distinguished limits and a particular choice for P,

$$\mathcal{F}_{\rm CH}(u) := \int\limits_\Omega \frac{1}{2}\left(\varepsilon^2 \Delta u - W'(u;\tau)\right)^2 - \varepsilon^p \left(\frac{\varepsilon^2 \eta_1}{2}|\nabla u|^2 + \eta_2 W(u)\right) dx. \tag{2.11}$$

The functionalization terms, parameterized by $\eta_1 > 0$ and $\eta_2 \in \mathbb{R}$, are analogous to the surface and volume energies typical of models of charged solutes in confined domains, see [Scherlis et al (2006)] and particularly equation (67) of [Andreussi et al (2012)]. The minus sign in front of η_1 is of considerable significance – it incorporates the propensity of the amphiphilic surfactant phase to drive the creation of interface. Indeed, experimental tuning of solvent quality shows that morphological instability in amphiphilic mixtures is associated to (small) negative values of surface tension, [Zhu et al (2009)] and [Zhu & Hayward (2012)]. In the FCH energy the gradient term, $-\eta_1|\nabla u|^2 < 0$, is localized on interfaces, associated to single-layers of surfactant molecules, whose growth lowers overall system energy – however the effect is *perturbative* and unrestricted growth is arrested by the penalty nature of the square term which keeps u close to the critical points of $\mathcal{E}_{\rm CH}$. The two distinguished limits correspond to difference choices for the exponent p in the functionalization terms. In the Strong Functionalization, $p = 1$, the functional terms dominate the Willmore corrections from the squared variational term. The Weak Functionalization, corresponding to $p = 2$, is the natural scaling for the Γ-limit as the curvature-type Willmore terms appear at the same asymptotic order as the functional terms.

The well-posedness of the minimization problem for the FCH, including the existence of global minimizers for fixed values of $\varepsilon > 0$ was established in [Promislow & Zhang (2013)] for a more general functional form over various natural function spaces. Depending upon the application, the volume-type η_2 functionalization perturbation incorporates the impact of counter-ion entropy (PEM fuel cells), capillary pressure, or entropic effects from constraint of tail groups (lipid bilayers), [Gavish et al (2012)]. The form $\eta_2 W(u)$ is chosen primarily for convenience, as integrals of $W(u)$ evaluated at critical points of $\mathcal{E}_{\rm CH}$ grow increasingly negative with increasing interfacial co-dimension. We remark that the surface term $\eta_1|\nabla u|^2$ is equivalent to an $\eta_1 u W'(u)$ functional-form since an integration by parts on $-\eta_1|\nabla u|^2$ yields $\eta_1 u\Delta u$ which can be absorbed into the squared variation with a perturbed form of W.

The goal of this survey is to present an overview of the stability and dynamics of classes of quasi-minimizer network morphologies $\mathcal{N}$ of $\mathcal{F}_{CH}$, which we define to be functions $u \in H^2(\Omega)$ which have an asymptotically small minority of amphiphilic phase, satisfy assigned boundary conditions, and render the free energy sufficiently small. Specifically for each fixed $C > 0$ we define the set of quasi-minimizing network morphologies

$$\mathcal{N}_C := \left\{ u \in H^2(\Omega) \Big| \int_\Omega |u - b_-|\, dx \le C\varepsilon \text{ and } \mathcal{F}_{CH}(u) \le C\varepsilon^{p+1} \right\}, \tag{2.12}$$

where the value of $\mathcal{F}_{CH}(u)$ can be negative.

3 Critical Points of the Functionalized Cahn-Hilliard Free Energy

For simplicity, we focus on the strong FCH, whose critical points, subject to a total mass constraint, are the solutions of the associated Euler-Lagrange equation

$$\frac{\delta \mathcal{F}}{\delta u} := \left(\varepsilon^2 \Delta - W''(u)\right)\left(\varepsilon^2 \Delta u - W'(u)\right) - \varepsilon\left(-\varepsilon^2 \eta_1 \Delta u + \eta_2 W'(u)\right) = \lambda, \tag{3.1}$$

e:FCH-cp

where $\lambda \in \mathbb{R}$ is the Lagrange multiplier. Intuitively, solutions of the critical point equation which are close to global minima of the FCH should also be close to critical points of the Cahn-Hilliard free energy, solving

$$\frac{\delta \mathcal{E}}{\delta u} := -\varepsilon^2 \Delta u + W'(u) = O(\varepsilon). \tag{3.2}$$

This observation further suggests that the Langange multiplier should scale with ε, that is $\lambda = \varepsilon \hat{\lambda}$, and we may rewrite the critical point equation as two, coupled second order systems

$$\begin{aligned} \varepsilon^2 \Delta u - W'(u) &= \varepsilon v, \\ \left(\varepsilon^2 \Delta - W''(u)\right) v &= \left(-\varepsilon^2 \eta_1 \Delta u + \eta_2 W'(u)\right) + \hat{\lambda}. \end{aligned} \tag{3.3}$$

e:FCH-cps

The singularly perturbed nature of the Euler-Lagrange system makes it amenable to dimensional reduction, yielding localized solutions build upon immersions in $\mathbb{R}^3$ of different co-dimensions. We first consider co-dimension one immersions, which we dress into bilayer morphologies which are quasi-minimizer of $\mathcal{F}_{CH}$. The first step in the dressing process is to produce a local coordinate system. More specifically, given a smooth, closed two-dimensional manifold Γ_b embedded in $\Omega \subset \mathbb{R}^3$, the "whiskered" coordinate is system defined in a tubular neighborhood of Γ_b via the mapping

$$x = \rho(s, z) := \zeta_b(s) + \varepsilon \nu(s) z, \tag{3.4}$$

where $\zeta_b : S \mapsto \mathbb{R}^3$ is a local parameterization of Γ_b and $\nu(s)$ is the outward unit normal to Γ. The variable z is often called the ε-scaled, signed distance to Γ, while the variables $s = (s_1, s_2)$ parameterize the tangential directions of Γ. In general it is the number of normal directions, the co-dimension, of the manifold which determines the stability properties of the associated dressing. We define an admissible class of co-dimension one interfaces, whose dressings will be quasi-minimizer of $\mathcal{F}_{CH}$.

issible **Definition 3.1 [Hayrapetyan & Promislow (2014)]** *For any $K, \ell > 0$ the family, $\mathcal{G}_{K,\ell}$, of "admissible interfaces" is comprised of closed (compact and without boundary), oriented 2 dimensional manifolds Γ embedded in $\mathbb{R}^3$, which are far from self-intersection and with a smooth second fundamental form. More precisely,*

(i) The $W^{4,\infty}(S)$ norm of the 2nd Fundamental form of Γ and its principal curvatures are bounded by K.

(ii) The whiskers of length $3\ell < 1/K$, in the unscaled distance, defined for each $s_0 \in S$ by, $w_{s_0} := \{x : s(x) = s_0, |z(x)| < 3\ell/\varepsilon\}$, neither intersect each-other nor $\partial\Omega$ (except when considering periodic boundary conditions).

(iii) The surface area, $|\Gamma|$, of Γ is bounded by K.

We will denote an admissible co-dimension one manifold by Γ_b, the 'b' is for bilayer. The associated change of variables $x \to \rho(s, z)$ is a C^4 diffeomorphism on the "reach",

$$\Gamma_b^\ell := \left\{ \rho(s, z) \in \mathbb{R}^d \,\middle|\, s \in S, -\ell/\varepsilon \le z \le \ell/\varepsilon \right\} \subset \Omega, \tag{3.5}$$

whiskNbd

of Γ_b. The white region in Figure 3.1 (right) depicts the reach of the associated immersion Γ_b.

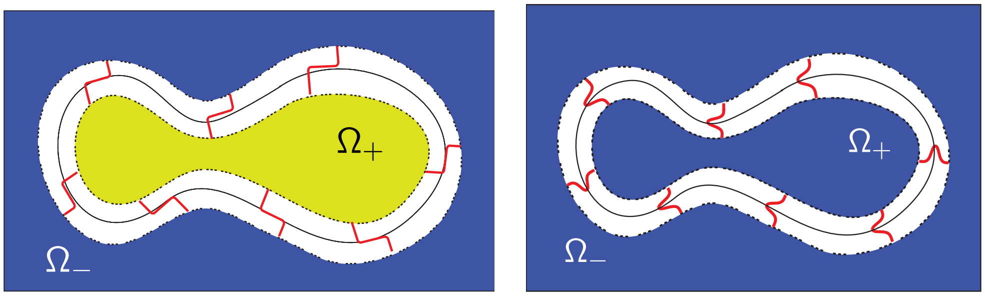

Figure 3.1: Single layer and Bilayer solutions of the Euler-Lagrange equation associated to the interface Γ. For the single layer solution Γ separates regions $u = b_-$ from $u = b_+$, while the bilayer solution corresponds to
solution $u = b_-$ on either side of the bilayer, with a brief excursion $u > b_-$ near Γ.

In the whiskered coordinates the Cartesian Laplacian takes the form

$$\varepsilon^2\Delta_x = \partial_z^2 + \varepsilon\partial_z J/(\varepsilon J)\partial_z + \varepsilon^2 J^{-1}\sum_{i,j=1}^{2}\frac{\partial}{\partial s_i}G^{ij}J\frac{\partial}{\partial s_j} = \partial_z^2 + \varepsilon H(s,z)\partial_z + \varepsilon^2\Delta_G, \tag{3.6}$$

where J is the Jacobian of the change of variables, $H = \partial_z J/(\varepsilon J)$ is the extended curvature, and $\mathbf{G} = G_{ij}$ is the metric tensor, see Section 6 of [Hayrapetyan & Promislow (2014)] for details tailored to the context of the FCH free energy. In particular, at leader order $H(s,z) = H_0(s) + O(\varepsilon z)$ where H_0 is the mean curvature of Γ_b at $\rho(s)$ and $\Delta_G = \Delta_s + O(\varepsilon z)$ where Δ_s is the usual Laplace-Beltrami operator on Γ_b.

In the whiskered coordinates the first equation of (3.3) reduces, at leading order to a second-order ODE in z, for the one-dimension profile $\phi(z)$,

$$\partial_z^2\phi(z) = W'(\phi), \tag{3.7}$$ e:BLcp

defined for $|z| \le \ell/\varepsilon$. Since the double-well W is assumed to have unequal depth wells $0 = W(b_-) > W(b_+)$, a simple phase-plane analysis shows that this equation supports a unique solution ϕ_b which is *homoclinic* to b_-, that is $\phi_b(z) \to b_-$ as $z \to \pm\infty$, see [Kapitula and Promislow (2013)] for a detailed analysis of the existence and linear analysis stability for homoclinic waves. We define the leading-order structure of the bilayer critical point, $u_b = u_b(x;\Gamma_b)$ as the bilayer "dressing" of Γ_b with ϕ_b,

$$u_b(x) := \phi_b(z(x)) + O(\varepsilon), \tag{3.8}$$ e:BL

for $x \in \Gamma_b^\ell$ and smoothly extend u_b to equal b_- off of Γ_b^ℓ, see Figure 3.1. We remark that if $g = g(z)$ decays exponentially to zero in z then $g \in L^2(\mathbb{R})$ and g has an extension $\tilde{g} \in L^2(\Omega)$ defined by $\tilde{g}(x) = g(z(x))$ on the reach of Γ_b and smoothly extended to zero off the reach. By abuse of notation, we use g to denote both the original function and its extension, in particular using both $\|g\|_{L^2(\mathbb{R})}$ and $\|g\|_{L^2(\Omega)}$ where the meaning is made clear by choice of inner product.

The $O(\varepsilon)$ correction, $u_{b,1}$ to u_b also plays a fundamental role, it is straight forward to see that is should solve

$$L_0 u_{b,1} = L_0^{-1}\left(-\eta_1\phi_b'' + \eta_2 W'(\phi_b) + \hat{\lambda}\right) + H_0(s)\phi_b', \tag{3.9}$$ e:BLcp1

where we introduce the Sturm-Liouville operator

$$L_0 := \partial_z^2 - W''(\phi_b), \tag{3.10}$$ e:L0-def

which is the linearization of (3.7) about ϕ_b. However there is a complication, whose resolution requires an understanding of the spectral properties of L_0 acting on an "infinite" whisker, that is on $L^2(\mathbb{R})$.

The translational invariance of the critical point equation (3.7) forces $L_0\phi_b' = 0$, and since ϕ_b is homoclinic its derivative has a zero at $z = 0$. By the Sturm-Liouville theory, $\psi_1 := \phi_b'$ is the first excited state (eigenmode) of L_0 acting on $L^2(\mathbb{R})$ with eigenvalue $\lambda_1 = 0$, and there exists a ground state eigenmode ψ_0 with no zeros, and eigenvalue $\lambda_0 > 0$. The remainder of the spectrum of L_0 is strictly negative. It is easy to see that the terms acted upon by L_0^{-1} in (3.9) are $L^2(\mathbb{R})$ orthogonal to ψ_1, and hence lie in the range of L_0. However for each fixed value of s, the term $H_0(s)\phi_b'$ is not orthogonal to ψ_1. Nevertheless, in [Doelman et al (submitted)] it is shown that exact critical points can be constructed for flat interfaces, where $H_0 \equiv 0$ and for constant curvature interfaces if λ is appropriately tuned. However we may construct quasi-minimizers of $\mathcal{F}_{CH}$ by dropping the curvature term in the construction of u_b. It will be accounted for later as a driving force for the geometric evolution of the underlying co-dimension one immersion Γ_b. Proceeding, we drop the curvature term, invert L_0 and decompose $u_{b,1}$ into a local term $\phi_{b,1}$ which decays exponentially to zero in z, and is smoothly extended to be zero off of Γ_b^ℓ, and a constant term

$$\gamma_1 = \frac{\hat{\lambda}_1}{\alpha_-^2}, \tag{3.11}$$ e:gam1-def

where we introduce the far-field well coercivity $\alpha_- := W''(b_-) > 0$. Consequently u_b admits the qausi-steady expansion

$$u_b(x) = \phi_b(z) + \varepsilon\left(\gamma_1 + \phi_{b,1}(z)\right) + O(\varepsilon^2). \tag{3.12}$$ ub-dressing

The local term $\phi_{b,1}$ corrects the structure of ϕ_b within the reach, while the spatial constant γ_1 adjusts the far-field behavior of u_b, which is now $b := b_- + \varepsilon\gamma_1 + O(\varepsilon^2)$. It is γ_1 that plays a key role in the evolution and bifurcation of the quasi-steady interfaces. Indeed this is the parameter Szostak tweaked when adding oleo-lipids to the bulk solvent phase.

Momentarily setting aside the mass constraint, there are two classes of free parameters in our construction of u_b, the spatially constant background correction, γ_1, and the interface shape Γ_b. It is instructive to examine the value of the FCH energy over the assocaited families of bilayer dressings, u_b, in particular the relation between the interface size and the total mass of available lipid. We first evaluate the free energy, which takes the form

$$\mathcal{F}(u_b) = \int_\Omega \frac{1}{2}\left(\varepsilon^2\Delta u_b - W'(u_b)\right)^2 - \varepsilon\left(\frac{\varepsilon^2\eta_1}{2}|\nabla u_b|^2 + \eta_2 W(u_b)\right)dx, \tag{3.13}$$

and break the integral over the near-field Γ_b^ℓ and far-field $\tilde{\Gamma}_\ell := \Omega\backslash\Gamma_b^\ell$. Denoting the near-field integral by $\mathcal{F}_\ell(u_b)$ we change to local coordinates

$$\begin{aligned}\mathcal{F}_\ell(u_b) &= \int_{\Gamma_b^\ell} \left(\varepsilon^2\Delta u_b - W'(u_b)\right)^2 - \varepsilon\left(\frac{\varepsilon^2\eta_1}{2}|\nabla u_b|^2 + \eta_2 W(u_b)\right)dx,\\ &= \int_{\Gamma_b}\int_{-\ell/\varepsilon}^{\ell/\varepsilon} \frac{1}{2}\left(\partial_z^2\phi_b - W'(\phi_b) + \varepsilon H_0(s)\partial_z\phi_b\right)^2 - \varepsilon\left(\frac{\eta_1}{2}|\partial_z\phi_b|^2 + \eta_2 W(\phi_b)\right) J(s,z)\,dz\,ds,\end{aligned} \tag{3.14}$$

where the Jacobian takes the form $J = \varepsilon + \varepsilon^2 z H_0(s) + O(\varepsilon^3 z^2)$. Expansing the Jacobian and keeping only leading order terms we find

$$\mathcal{F}_\ell(u_b) = \varepsilon\int_{\Gamma_b}\int_{-\ell/\varepsilon}^{\ell/\varepsilon} \frac{\varepsilon^2}{2}\left(L_0(\gamma_1 + \phi_{b,1}) + H_0(s)\phi_b'\right)^2 - \varepsilon\left(\frac{\eta_1}{2}|\phi_b'|^2 + \eta_2 W(\phi_b(z))\right)ds\,dz. \tag{3.15}$$

The localized functions in the squared term will yield $O(\varepsilon^3)$ integrals which are negligible. Moreover integrating (3.7) we see that $(\phi_b')^2 = 2W(\phi_b)$. Together these two observations allow us to rewrite the localized component of the free energy as,

$$\mathcal{F}_\ell(u_b) = \varepsilon^2 |\Gamma_b| \left(\ell \gamma_1^2 \alpha_-^2 - \frac{\eta_1 + \eta_2}{2} \sigma_b \right), \tag{3.16}$$

where we introduced the bilayer 'surface tension' $\sigma_b := \|\phi_b'\|^2_{L^2(\mathbb{R})}$. In the far-field region u_b takes the spatially constant value

$$u_b(x) = b := b_- + \varepsilon\gamma_1 + O(\varepsilon^2), \qquad x \in \tilde{\Gamma}_\ell, \tag{3.17}$$ b-def

for which value $W'(b) = \varepsilon\alpha_-\gamma_1 + O(\varepsilon^2)$, and $W(b) = O(\varepsilon^2)$. The far-field contribution to the energy thus reduces to the leading order expression,

$$\tilde{\mathcal{F}}_\ell(u_b) = \varepsilon^2(|\Omega| - 2\ell|\Gamma|)\frac{1}{2}\gamma_1^2\alpha_-^2 + O(\varepsilon^3). \tag{3.18}$$

Combining the near- and far-field expressions, the total energy takes the form

$$\mathcal{F}(u_b) = \varepsilon^2 \left(\frac{\alpha_-^2 |\Omega|}{2} \gamma_1^2 - |\Gamma_b| \frac{\eta_1 + \eta_2}{2} \sigma_b \right). \tag{3.19}$$ e:TFc

A similar decomposition of the integrals shows that the total mass of amphiphilic material is

$$M := \int_\Omega u_b(x)\, dx = \int_\Omega (b + u_b - b)\, dx = |\Omega|(b_- + \varepsilon\gamma_1) + \varepsilon|\Gamma_b| m_b, \tag{3.20}$$

where $m_b := \int_{\mathbb{R}} \phi_b(z) - b_-\, dz > 0$, is the mass of amphiphilic material per unit length of bilayer. Typically the amphiphilic component is scarce within the bulk, so that $M = \varepsilon\hat{M}$ (don't put too much soap in the washing machine!), and since Γ_b is admissible its interfacial area $|\Gamma_b|$ is $O(1)$. These assumptions render u_b a quasi-minimizer of $\mathcal{F}_{CH}$, moreover a prescribed value of $\hat{M}$ and γ_1 determines the area $|\Gamma_b|$ of the bilayer interface. Consequently, the minimization of $\mathcal{F}(u_b)$ over Γ_b and γ_1, subject to the mass constraint reduces to a the optimization of a quadratic polynomial in γ_1 which yields the optimal value

$$\gamma_b^* = -\frac{\eta_1 + \eta_2}{2} \frac{\sigma_b}{m_b \alpha_-^2}, \tag{3.21}$$ e:gamma1-def

of amphiphilic material in the bulk region. For the strong functionalization only the area of an admissible co-dimension one interface, and not its curvature, enter into the leading-order determination of the free energy of its bilayer dressing. Moreover bilayers prefer an optimal far-field value of lipid, γ_b^* which is independent of the scaled mass constraint $\hat{M}$ and hence the area of the bilayer – it is a universal property of the system as determined by the shape of the well W throughout m_b, σ_b, and α_- and through the functionalization parameters η_1 and η_2. For the weak functionalization the Willmore term, the integral of the square of the mean curvature over Γ_b, enters into the free energy at leading order, and the optimization is more subtle.

There are critical points of $\mathcal{F}$ for which λ is $O(1)$, in particular the *single-layer* solutions, which correspond to heteroclinic orbits of (3.7) that connect two equilibrium values, see Figure 3.1 (left). For the Cahn-Hilliard free energy single-layers form the dominant global minimizers, however they are generically saddle points of the FCH, and are susceptible to meander instabilities in the gradient flow, as discussed below. It is important to emphasize that single-layers and bilayers are distinct morphologies – single-layers separate phase A from phase B while bilayers separate phase A into two regions by a thin layer of phase B, see Figure 3.1. In particular bilayers can rupture, re-uniting the two regions of phase A, as when a lipid bilayer opens a pore, or tears. In addition, the interfacial component is a conserved quantity for bilayers, and when the bilayer is stretched the interface must

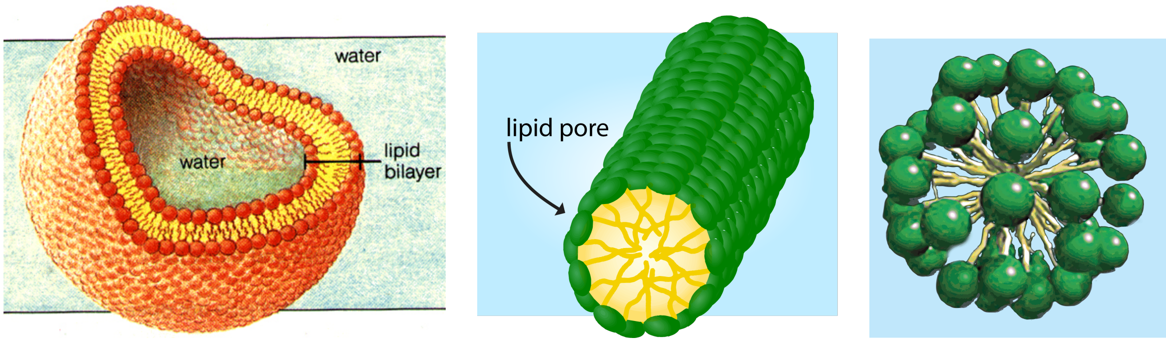

Figure 3.2: Depiction of bilayer (left, source: *academic.brooklyn.cuny.edu*), pore (center), and micelle (right) morphologies of lipids. The co-dimension associated to the morphology is the difference between the space dimension and the number of tangent directions of the minimal manifold whose normal bundle locally foliates the morphology. In $\mathbb{R}^3$ bilayers are co-dimension one, pores are co-dimension two, and micelles are co-dimensionl three.

etworks

thin, which naturally increases its free energy as it deforms from its equilibrium profile ϕ_b – bilayers can support non-zero tangential stresses.

The FCH critical point equation also possesses co-dimension two solutions in $\mathbb{R}^3$. These are based upon a foliation of a neighborhood of a smooth, closed, non-self intersecting one dimensional manifold Γ_p immersed in Ω. The local coordinate system takes the form

$$x = \rho_p(s, z_1, z_2) = \zeta_p(s) + \varepsilon \left(z_1 N_1(s) + z_2 N_2(s) \right), \tag{3.22}$$

where N_1 and N_2 are orthogonal unit vectors which are also orthogonal to the tangent vector $\zeta_p'(s)$. Within the reach Γ_p^ℓ of Γ_p the Laplacian admits the local form

$$\Delta_s = \Delta_R + \varepsilon \vec{\kappa}(s, z) \cdot \nabla_z + \varepsilon^2 D_s^2, \tag{3.23}$$

where Δ_R is the usual cylindrical Laplacian in (R, Θ) which correspond to the scaled normal distances $\vec{z} = (z_1, z_2)$, $\vec{\kappa} = (\kappa_1, \kappa_2)^T$ are the two curvatures of Γ_p at $\zeta_p(s)$, and D_s^2 reduces to the line diffusion operator on Γ_p when $\vec{z} = 0$, see [Dai & Promislow (submitted)] for details. Assuming axial symmetry, the leading order pore profile associated to the critical point equation (3.1) satisfies co-dimension two critical point equation

$$\partial_R^2 \phi_p + \frac{1}{R} \partial_R \phi_p = W'(\phi_p), \tag{3.24}$$ e:P-cp

subject to $\partial_R \phi_p(0) = 0$ and $\phi_p \to b = b_- + \varepsilon \gamma_1 + O(\varepsilon^2)$ as $R \to \infty$. The leading order form for the pore quasi-minimizer network arises from the pore profile dressing of a co-dimension two interface Γ_p,

$$u_p(x) := \phi_p(R(x)) + \varepsilon \left(\gamma_1 + \phi_{p,1}(R) \right) + O(\varepsilon^2), \tag{3.25}$$ up-dressing

It is also possible to combine bilayer and pore quasi-minimizer, so long as the associated manifolds have non-intersecting reaches, *and* the far-field constant γ_1 takes a common value. Indeed, the quasi-steady evolution between co-existing co-dimension one and co-dimension two interfaces is driven by the competition between this common far-field value b. If the optimal far-field values associated to distinct co-dimensional morphologies differ, then the morphologies will not coexist over long time periods; one will grow on a slow time scale at the expense of the other, as described in section 5.

Micelle, or co-dimension three solutions of the critical point equation reduce, in $\mathbb{R}^3$, to solutions of the usual spherical Laplacian. Assuming rotational symmetry, the leading order micelle profile is the

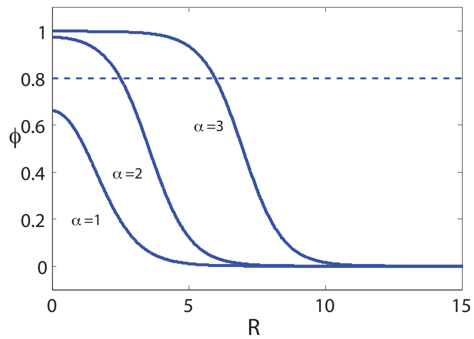

M_n^{core} (g/mol)	2500 ± 40	5850 ± 204
bilayer	8.7 ± 1.2	15.8 ± 2.8
pore	14.3 ± 1.6	25.4 ± 3.3
micelle (nm)	18.4 ± 2.6	38.8 ± 10.2

Figure 3.3: (left) A comparison of co-dimension $\alpha = 1, 2$, and 3 profiles computed from (3.7), (3.24), and (3.26) respectively. The relative widths the profile is most sensitive to the difference in depths of the two wells: $W(b_-) - W(b_+) > 0$. (right) A table of experimental data, from [Jain & Bates (2004)], indicating radii of bilayer, pore, and micelle morphologies obtained by varying the hydrophilic length of polymer in PEO-PB amphiphilic di-blocks with fixed hydrophobic (core) molecule weight, M_n^{core}, as indicated. f:Jain

unique solution of

$$\partial_R^2 \phi_m + \frac{2}{R} \partial_R \phi_m = W'(\phi_m), \tag{3.26}$$

e:M-cp

subject to $\partial_R \phi_m(0) = 0$ and $\phi_m \to b$ as $R \to \infty$. A key prediction of the FCH free energy is that bilayers must be thinner than pores, which in turn are thinner than micelles. This observation is born out by experimental data, Figure 3.3 (right).

4 Network Bifurcation in the FCH

The quasi-minimizer network morphologies developed in section 3 are, at leading order, critical points of the Cahn-Hilliard, however these structures are not close to local minima but are rather quasi-saddle points of the CH free energy. An essential feature of the functional form of the FCH is its facility to build local minima out of the saddle points of the simpler CH free energy. This process is best understood by examining the second variational derivative of the FCH free energy at a smooth critical point, u_c of the Cahn-Hilliard free energy. For traceless boundary conditions, such as periodic boundary conditions, see [Promislow & Zhang (2013)] for a detailed discussion of appropriate boundary conditions, then the second variation takes the form

$$\mathbb{L}_{u_c} := \frac{\delta^2 \mathcal{F}}{\delta u^2}(u_c) = \left(\varepsilon^2 \Delta - W''(u_c)\right)^2 - \varepsilon^p \left(\eta_1 \varepsilon^2 \Delta + \eta_2 W''(u_b)\right). \tag{4.1}$$

For the bilayer quasi-minimizer, u_b, associated to an admissible, co-dimension one interface Γ_b, the second variational derivative $\mathbb{L}_b := \mathbb{L}_{u_b}$, takes a simplified form when acting on functions $u \in H^4(\Omega)$ whose support lies within the reach, Γ_b^ℓ, of Γ. On this subspace the operator admits the asymptotic expansion

$$\mathbb{L}_b = \left(L_0 + \varepsilon H \partial_z + \varepsilon^2 \Delta_s\right)^2 - \varepsilon^p \left(\eta_1 \partial_z^2 + \eta_2 W''(\phi_b)\right) + O(\varepsilon^{p+1}), \tag{4.2}$$

e:Lb-def

and the leading order structure of $\mathbb{L}_b$ is controlled by $\mathcal{L}^2$ where $\mathcal{L} := L_0 + \varepsilon^2 \Delta_s$ is the dominant part of the second variation of $\mathcal{E}$ at u_b. The remaining parts of $\mathbb{L}_b$ are relatively bounded and asymptotically small in comparison to $\mathcal{L}^2$.

The spectrum of the operator $\mathbb{L}_b$ can be built from the spectrum of its constituents L_0 and Δ_s. The spectral properties of L_0 are described in section 3 and depicted in Figure 4.1 (left). The Laplace-Beltrami operator Δ_s is self-adjoint over $L^2(\Gamma)$ where, for each admissible interface Γ, the inner

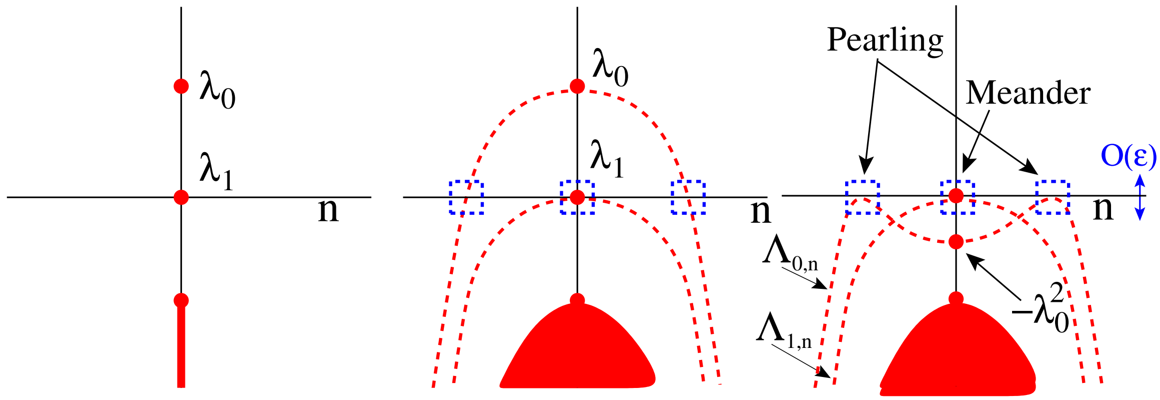

Figure 4.1: The structure of the real spectrum of $-\mathbb{L}_b$ plotted verses Laplace-Beltrami wavenumber n. (left) The Sturm-Liouville operator L_0, defined in (3.10), has one positive ground state eigenvalue, $\lambda_0 > 0$ and a one dimensional kernel, denoted λ_1. (center) The extension of L_0 to $\mathcal{L} = L_0 + \varepsilon^2 \Delta_s$ adds side-bands in n, the Laplace-Beltrami index which bend back negatively at the rate $-(\lambda_0 - \varepsilon^2 \beta_k)^2$. (right) The spectrum of the operator $-\mathbb{L} = -\mathcal{L}^2 + O(\varepsilon)$, (minus sign chosen to preserve orientation of images) is, to $O(\varepsilon)$, the negative square of the spectrum of $\mathcal{L}$. The side-band associated to λ_0 has a quadratic tangency at leading order, which may be raised or lowered by the functional terms, η_1 and η_2, the crossing of this spectrum through zero is the mechanism of the pearling instability.

Spectrum

product is defined by

$$\langle f, g \rangle_{L^2(\Gamma)} := \int_\Gamma f(s) g(s) J_0(s)\, ds, \tag{4.3}$$

where $J_0 = \sqrt{\mathbf{g}}$ is the square root of the determinant of the first fundamental form of Γ. The eigenvalues $\{\beta_n\}_{n=0}^\infty$ of $-\Delta_s$ may be enumerated in increasing size with $\beta_0 = 0$ and $\beta_1 > 0$. The associated Laplace-Belrami eigenmodes $\{\Theta_n\}_{n=0}^\infty$ are orthonormal in the $L^2(\Gamma)$ norm.

Theorem 4.1 (Weyl asymptotics [Chavel I.(1984)]) *Let Γ_b be an admissible co-dimension one interface immersed in $\mathbb{R}^d$, and let $N(x)$ denote the number of eigenvalues of $-\Delta_s$, counted according to multiplicity, that are smaller than x, then*

$$N(x) \sim C x^{\frac{d-1}{2}}. \tag{4.4}$$

In particular, $\beta_n \sim \tilde{C} n^{\frac{2}{d-1}}$.

Indeed, in [Hayrapetyan & Promislow (2014)] it was shown that for each admissible class, $\mathcal{G}_{k,\ell}$, of co-dimension one interfaces there exists $U > 0$, which may be chosen independent of $\varepsilon > 0$ such that the eigenfunctions associated to $\mathbb{L}_b$ with corresponding to eigenvalues $\lambda < U$ comprise two sets, the *pearling eigenmodes* $\{\Psi_{0,n}\}_{n=N_1}^{N_2}$ and the *meander eigenmodes* $\{\Psi_{1,n}\}_{n=0}^{N_3}$ and moreover these eigenmodes admit the asymptotic form

$$\Psi_{j,n} = \psi_j(z)\Theta_n(s) + O(\varepsilon), \tag{4.5}$$

for $j = 0, 1$ and n running over the corresponding indices. For $j = 0, 1$ we introduce Σ_j, the set of indices n for which $\mathbb{L}_b$ acting on $\psi_j \Theta_n$ is small, i.e.,

$$\Sigma_j := \{n \mid (\lambda_j - \varepsilon^2 \beta_n) \sim O(\sqrt{\varepsilon})\}. \tag{4.6}$$

From Weyl's asymptotic formula we deduce that $|\Sigma_0| \sim O(\varepsilon^{3/2-d}) \gg 1$. For the strong functionalization, $p = 1$, we look for an expression of the pearling eigenvalues in order to determine a condition for pearling stability. For Γ_b an admissible co-dimension one interface we consider the eigenvalue problem

$$\mathbb{L}_b \Psi_{0,n} = \Lambda_{0,n} \Psi_{0,n}, \tag{4.7}$$

associated to the second variation of $\mathcal{F}_{CH}$ about the bilayer dressing u_b. The spectrum of $\mathbb{L}_b$ cannot be localized by a regular perturbation expansion since the eigenvalues are asymptotically close together. We need bounds on the spectrum that are uniform in $\varepsilon \ll 1$. To this end we introduce the $L^2(\Omega)$ orthogonal projection Π onto the space

$$X_b := \mathrm{span}\{\psi_{\mathrm{j}}(\mathrm{z})\Theta_{\mathrm{n}}(\mathrm{s}) \big| \, \mathrm{j} = 0, 1, \text{ and } \mathrm{n} \in \Sigma_{\mathrm{j}} \text{ respectively}\}, \tag{4.8}$$

which approximates the eigenspaces of $\mathbb{L}_b$ corresponding to pearling ($j = 0$) and meander ($j = 1$) eigenmodes. Functionally, Π, acts on $f \in L^2(\Omega)$ by

$$\Pi f := \sum_{k \in \Sigma_0} \langle f, \psi_0 \Theta_k \rangle_{L^2(\Omega)} \psi_0 \Theta_k + \sum_{k \in \Sigma_1} \langle f, \psi_1 \Theta_k \rangle_{L^2(\Omega)} \psi_1 \Theta_k, \tag{4.9}$$

with its complementary projection denoted $\tilde{\Pi} := I - \Pi$. We decompose the operator $\mathbb{L}_b$ into a 2×2 block form using the projections

$$\tilde{\mathbb{L}}_b := \begin{bmatrix} \Pi \mathbb{L}_b \Pi & \Pi \mathbb{L}_b \tilde{\Pi} \\ \tilde{\Pi} \mathbb{L}_b \Pi & \tilde{\Pi} \mathbb{L}_b \tilde{\Pi} \end{bmatrix}. \tag{4.10}$$

The upper-left element $\Pi \mathbb{L}_b \Pi$ can be written as a matrix $M \in \mathbb{R}^{N \times N}$ where $N \approx \varepsilon^{3/2-d}$ has entries

$$M_{j,k} := \langle \mathbb{L}_b \psi_0 \Theta_j, \psi_0 \Theta_k \rangle_{L^2(\Omega)}. \tag{4.11}$$ e:Mjk-def

The off-diagonal terms are small, in norm, and the spectrum of the fully infinite dimensional piece, $\tilde{\Pi} \mathbb{L}_b \tilde{\Pi}$, is bounded from below by the aforementioned $U > 0$. We will show that the spectrum of $\mathbb{L}_b$ sufficiently below U is controlled by the spectrum of the matrix M which we characterize.

The matrix M has large dimension and hence care must be taken to distinguish between the size of the entries of M and the size of M as an operator. Indeed, the norm of a matrix as an operator from $l^2(\mathbb{R}^N)$ to $l^2(\mathbb{R}^N)$ generically scales like $\sqrt{N}$ times the l^∞ norm of its entries. However uniform norm bounds are possible, via a convolution style argument, if the off-diagonal elements decay sufficiently quickly.

volution **Lemma 4.2 [Kraitzman (thesis)]** *Fix $c > 0$ and assume that the entries of $A \in \mathbb{R}^{N \times N}$ satisfy the bound*

$$|A_{j,k}| \leq \frac{c}{1 + (k - j)^2}. \tag{4.12}$$

Then the matrix A is uniformly bounded from $l^2(\mathbb{R}^N)$ to $l^2(\mathbb{R}^N)$ independent of N.

Our goal is to show that the matrix M admits an admits an asymptotic decomposition

$$M = M^0 + \varepsilon^q \tilde{M}. \tag{4.13}$$

For values of $q > \frac{1}{4} + \frac{d}{2}$, if the entries of $\tilde{M}$ are uniformly bounded then there exists a constant $C > 0$, independent of ε such that $\varepsilon^q \|\tilde{M}\|_{L^2} \ll \varepsilon$. That is, it is sufficient to uniformly bound the entries of $\tilde{M}$ to see that $\varepsilon^q \tilde{M}$ acts as a lower-order perturbation on the eigenvalues of M. We will handle the matrix M^0 using Lemma 4.2, so long as the interface Γ_b is sufficiently smooth, as is guaranteed by its admissibility. For simplicity we focus only on the pearling modes $j = 0$, neglecting the meander terms associated to $j = 1$. Using the expansion (4.2) of $\mathbb{L}_b$ and recasting the inner product in (4.11) in terms of the whiskered coordinates, the diagonal terms of the matrix M^0, at leading order, take the form

$$M^0_{k,k} = (\lambda_0 - \varepsilon^2 \beta_k)^2 - \varepsilon(\gamma_1 \alpha_-^2 S + \lambda_0(\eta_1 - \eta_2)\|\psi_0\|_2^2), \tag{4.14}$$

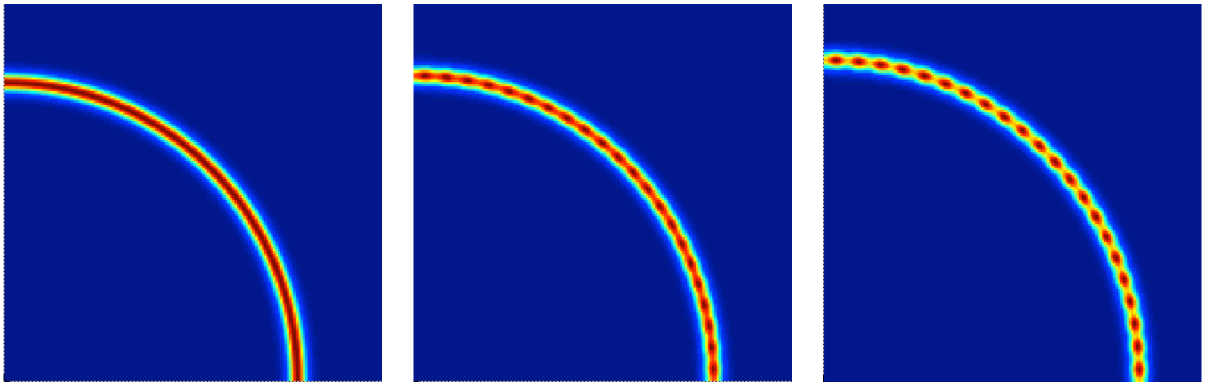

pearling

Figure 4.2: Time evolution of a circular, co-dimension one bilayer under the FCH gradient flow (5.1) for vales $\varepsilon = 0.1$ and $\eta_1 = \eta_2 = 2$. The times depicted correspond to $t = 0$, $t = 114$, and $t = 804$ and show the onset of the pearling bifurcation.

where the sign of the "shape factor"

$$S := \int_{\mathbb{R}} W'''(\phi_b)\psi_0^2(z) L_0^{-1} 1\, dz, \tag{4.15}$$

determines if the pearling bifurcation absorbs amphiphilic material from the bulk or releases it. For $k \in \Sigma_0$, the quadratic term is bounded by $O(\varepsilon)$ but becomes dominant as k approaches the boundary of the set Σ_0 of pearling indices. The off-diagonal terms of M^0 are formally lower order, admitting the expansion

$$M^0_{j,k} = -\varepsilon^2 \int_\Gamma (\sigma_b H_0^2 + S_1 H_1)\Theta_k \Theta_j J_0(s)\, ds, \tag{4.16}$$

where the coefficient $S_1 := \int_{\mathbb{R}} W'''(\phi_b)\phi_b' \psi_0^2 z\, dz$ and $H_1 = k_1^2 + k_2^2$ is the sum of the squares of the curvatures of Γ_b. However they form a lower order operator on $l^2(\mathbb{R}^N)$ only if we can apply Lemma 4.2. These estimates are achieved in [Kraitzman (thesis)], in particular it is shown that

Theorem 4.2 [Kraitzman (thesis)] *Let $\Gamma \subset R^d$ be an admissible interface, with curvatures $\vec{k} = (k_1, \cdots, k_{d-1})$ in $W^{4,\infty}(\Gamma_b)$ and $f : R^{d-1} \to R$ a smooth function. Then there exist constants $c_1, c_2, c > 0$ such that for every $k, j \in N,\ k \neq j$,*

$$\left| \int_\Gamma f(\vec{k})\Theta_k \Theta_j\, J_0 ds \right| \leq \frac{1}{\beta_k + \beta_j}\left(c_1 + c_2 \int_\Gamma \left| \Delta_s^{-1}(\nabla_s \Theta_k \nabla_s \Theta_j) \right|\, J_0 ds \right) \leq \frac{c}{1 + |k-j|^2}. \tag{4.17}$$

As a consequence, the matrix M^0 can be written as

$$M^0 = D + \varepsilon^2 A, \tag{4.18}$$

where D is a diagnonal matrix with entries

$$D_{k,k} = (\lambda_0 - \varepsilon^2 \beta_k)^2 - \varepsilon(\gamma_1 \alpha_-^2 S + \lambda_0(\eta_1 - \eta_2)||\psi_0||_2^2), \tag{4.19}$$

and A is uniformly bounded as an operator on $l^2(\mathbb{R}^N)$. Since $\varepsilon^q \tilde{M}$ is also lower order as an operator, the eigenvalues of M take the form

$$\Lambda_{0,n} = (\lambda_0 - \varepsilon^2 \beta_n)^2 - \varepsilon(\gamma_1 \alpha_-^2 S + \lambda_0(\eta_1 - \eta_2)\|\psi_0\|_2^2) + o(\varepsilon^2). \tag{4.20}$$

Weyl asymptotics imply that the separation between Laplace-Beltrami eigenvalues scales like $O(\sqrt{\varepsilon})$ for $\beta_n \approx \varepsilon^{-\frac{1}{2}}$, hence $\lambda_0 - \varepsilon^2\beta_k$ can be made as small as $O(\varepsilon)$. This shows that the squared term is lower order near the turning point of the pearling spectrum, see Figure 4.1 (right). Assuming that the shape factor $S < 0$, which is true for a genetic class of double-wells, W, see section 5 of [Doelman et al (submitted)], the spectrum of M will contain negative eigenvalues if and only if γ_1 satisfies the *pearling condition*

$$P_* := -\frac{\lambda_0(\eta_1 - \eta_2)\|\psi_0\|_{L^2}^2}{\alpha_-^2 S} > \gamma_1. \tag{4.21}$$

e:pearl-cond

To connect the spectrum of M to that of $\mathbb{L}_b$, we must bound the interaction between the projection Π and the operator $\mathbb{L}_b$. If Π where a spectral projection associated to $\mathbb{L}_b$ then the two operators would commute, and since $\Pi\tilde{\Pi} = 0$, the off-diagonal terms would be zero. However X_b only approximates a spectral subset of $\mathbb{L}_b$, and the estimates $\|\Pi\mathbb{L}_b\tilde{\Pi}\|_{L^2(\Omega)} = \|\tilde{\Pi}\mathbb{L}_b\Pi\|_{L^2(\Omega)} \leq C\varepsilon$, are sharp. However the restricted operator $\tilde{\Pi}\mathbb{L}_b\tilde{\Pi}$ is uniformly coercive on L^2 and with its spectrum is bounded from below by $U > 0$ which may be chosen independent of sufficiently small $\varepsilon > 0$. In this case, for any $\lambda < U$ we introduce $B := \Pi\mathbb{L}_b\tilde{\Pi}$ and $C := \tilde{\Pi}\mathbb{L}_b\tilde{\Pi}$ and reduce the 2×2 representation of the eigenvalue problem

$$\begin{bmatrix} M & B \\ B^T & C \end{bmatrix} \begin{bmatrix} v_1 \\ v_2 \end{bmatrix} = \lambda \begin{bmatrix} v_1 \\ v_2 \end{bmatrix} \tag{4.22}$$

to a finite dimensional system for the component v_1, which solves

$$(M - \lambda)v_1 = -B(C - \lambda)^{-1}B^T v_1. \tag{4.23}$$

In particular, taking the l^2 norm of both sides and using the estimates on B, B^T, and the distance of λ to $\sigma(C)$ to estimate the norm of the resolvent, we have

$$\|(M - \lambda)v_1\|_{l^2} \leq \frac{c\varepsilon^2}{|U - \lambda|}\|v_1\|_{l^2}. \tag{4.24}$$

For λ an order of one distance from ν this estimate implies that $\mathrm{dist}(\lambda, \sigma(M)) = O(\varepsilon^2)$, so that the spectrum of $\mathbb{L}_b$ below U lies within $O(\varepsilon^2)$ of the spectrum of M. In particular, if the spectrum of M is bounded from below by a positive $O(\varepsilon)$ quantity, then so is the spectrum of $\mathbb{L}_b$. Conversely, since $M_{k,k} = \langle \mathbb{L}_b\psi_0\Theta_k, \psi_0\Theta_k\rangle_{L^2(\Omega)}$ it follows from the variational characterization of the spectrum of $\mathbb{L}_b$ that the smallest eigenvalue of $\sigma(\mathbb{L}_b)$ is smaller (more negative) than the smallest diagonal element of M. We deduce from these calculations that the pearling condition (4.21) applies to $\mathbb{L}_b$. Moreover, this is in agreement with Szostak's experiment, the photo-induced increase in charge on the lipid heads induced a pearling bifurcation and drove pores to micelles. The increase in charge corresponds, within the FCH, to an instantaneous increase in η_1; a sufficiently large increase, for a fix value of γ_1, will trigger the pearling condition (4.21).

5 Competitive Geometric Evolution of Bilayers and Pores

The over damped dynamics of amphiphilic polymer suspensions can be received from the Functionalized Cahn-Hilliard free energy via its gradient flows whose evolution preserves the volume fraction of the constituent species and lowers the free energy. Similar to the Cahn-Hilliard gradient flow given in (2.4), the simplest mass preserving gradient flow of the FCH is generated by the H^{-1} gradient,

$$u_t = \Delta\frac{\delta\mathcal{F}}{\delta u} = \Delta\left[\left(-\varepsilon^2\Delta + W''(u) - \varepsilon\eta_1\right)\left(-\varepsilon^2\Delta u + W'(u)\right) + \varepsilon(\eta_1 - \eta_2)W'(u)\right]. \tag{5.1}$$

e:FCH-H1

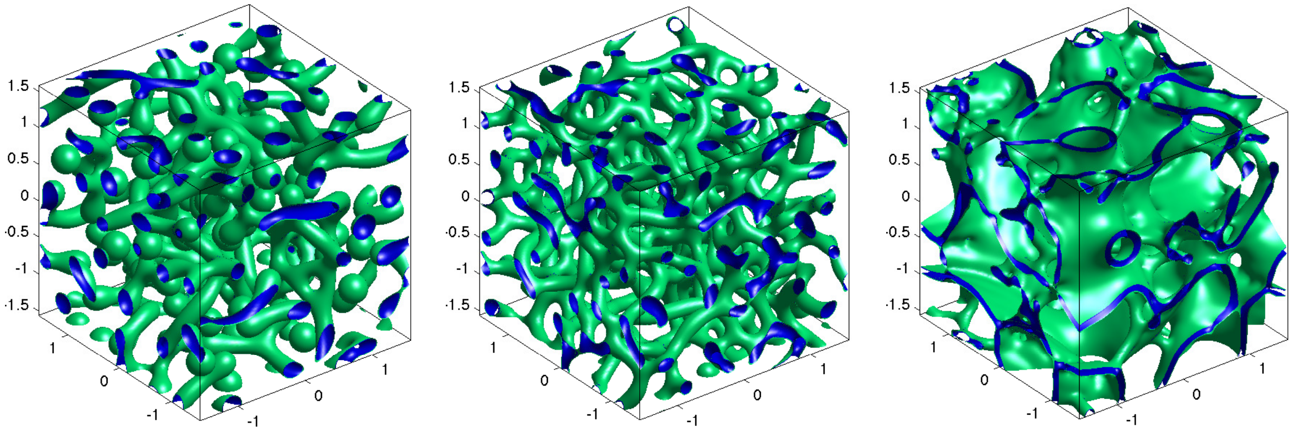

Figure 4.3: level sets $u = 0.4$ (green) and $u = 0.45$ (blue) of quasi-minimizers of the Functionalized Cahn-Hilliard free energy obtained from the mass preserving gradient flow (5.1) from identical initial data. The parameter values are $\varepsilon = 0.03$, $b_\pm = \pm 1$, the well satisfies $W(-1) = 0 > W(1) = -0.3$, $\eta_1 = 5$ and $\eta_2 = -2, 1$, and 5 in the panels from left to right, yielding micelles - pore, pore, and bilayer dominate networks respectively. Images courtesy of Andrew Christlieb and Jaylan Jones.

co-dims

The quasi-minimizer network morphologies constructed in section 3 are not stationary solutions of the FCH gradient flow, but generate slow dynamics which may be locally parameterized by the interfacial sub-manifolds of bilayers and pores, respectively Γ_b and Γ_p. Indeed, when the pearling condition does not hold, then meander eigenvalues associated to the bilayer morphologies span the tangent plane to the manifold of bilayer configurations, parameterized by the admissible interfaces. The flow of the underlying interfacial structure can be obtained by projecting the residual $\frac{\delta \mathcal{F}}{\delta u}(u_b)$ of the critical point equation (3.1) onto this tangent plane. The method of matched asymptotic expansion provides a more accessible, but formal method to derive the interfacial motion. For a bilayer morphology, the ansatz (3.12) for u_b is augmented by taking the signed distance z to the interface Γ_b and the background state γ_1 to be functions of the slow scaled time $t_1 = t/\varepsilon$, and the gradient flow is solved by matching fluxes, particularly across the interfacial layers. For single layer morphologies, under the Cahn-Hilliard gradient flow this results in a Mullins-Sekerka flow for the interface, see [Pego (1989)]. For the FCH gradient flow, (5.1) reduces, at leading order, to

$$\varepsilon \phi_b'(z) \frac{\partial z}{\partial t_1} + \varepsilon \frac{d\gamma_1}{dt_1} = \Delta \frac{\delta \mathcal{F}}{\delta u}(u_b) = \varepsilon \Delta H_0(s) \phi_b'(z) + O(\varepsilon^2). \tag{5.2}$$

The leading order residual arises from the mean-curvature term which was neglected in the construction of the bilayer, u_b. This term now becomes a driving force for the evolution of the interface Γ_b through the change in the signed distance function. Indeed, the quantity

$$V_b(s) := -\frac{\partial z}{\partial t_1}, \tag{5.3}$$

is the normal velocity of the interface Γ_b. The asymptotic reduction does lead to a Mullins-Sekerka problem for the far-field chemical potential, however its driving force is given by the interfacial mean curvature times the derivative of the bilayer profile at the interface, $H_0(s)\phi_b'(0)$. Since the bilayer is symmetric across the interface its derivative is zero, $\phi_b'(0) = 0$, and the Mullins-Sekerka problem is trivial. The outer chemical potential reduces to a spatial constant, and the far-field is characterized by amphiphilic density, $\gamma_1(t_1)$, whose value in determined by conservation of total mass, see [Dai & Promislow (2013)] for details for bilayers under the weak functionalization. For the strong

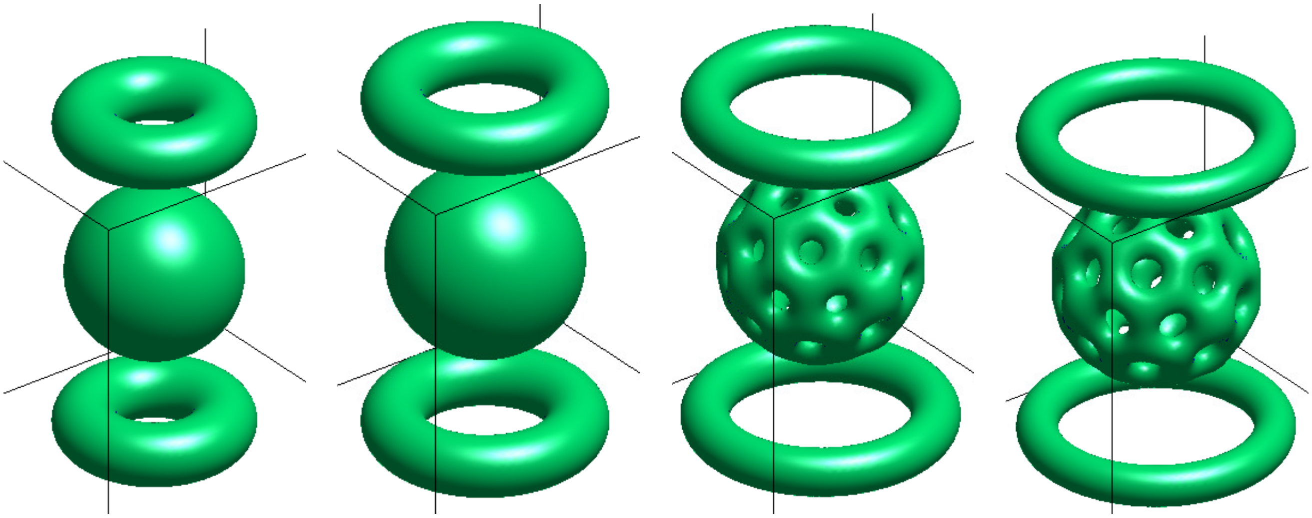

Figure 5.1: Competition for the amphiphilic phase between a spherical bilayer (beach ball) and circular solid pore (hula hoop) as a function of the well tilt $W(b_-) - W(b_+)$. The image shows $t = 100$ end states of the FCH gradient flow (5.1) from identical initial data but with increasing values of the well tilt. Small tilt prefers bilayers, larger tilt prefers pores by increasing γ_b^* and the pearling threshold, P_*, which drives bilayers to pearl. Images courtesy of Andrew Christlieb and Jaylan Jones.

petition

functionalization the resulting system takes the form

$$\begin{aligned} V_b &= \nu_b(\gamma_1 - \gamma_b^*) H_0, \\ \frac{d\gamma_1}{dt_1} &= -\nu_b m_b (\gamma_1 - \gamma_b^*) \int_{\Gamma_b} H_0^2 \, dS, \end{aligned} \tag{5.4}$$

e:BL-quenched

where $\nu_b := \frac{m_b}{\int_{\mathbb{R}} (\phi_b - b_-)^2 \, dz} > 0$ and γ_b^* is the optimal far-field amphiphilic density derived by the optimization process in (3.21). The H^{-1} gradient flow drives pure bilayer interfaces by a quenched mean-curvature flow. While the flow drives γ_1 to its optimal value γ_b^*, the sign of the difference $\gamma_1 - \gamma_b^*$ is consequential. Indeed, in two space dimension, modulo reparamerization of the evolving interface, the curvature driven flow can be recast as an evolution equation of the single curvature H_0,

$$\frac{\partial H_0}{\partial t_1} = -(\partial_s^2 + H_0^2) V_b = \nu_b(\gamma_1 - \gamma_b^*)(\partial_s^2 + H_0^2) H_0, \tag{5.5}$$

see section 3.3 of [Gavish et al (2011)] for details. If $\gamma_1 > \gamma_b *$, that is if the bulk value of amphiphilic material is in excess then the curvature driven flow is a backwards-heat equation in the curvatures. This is the nature of the fingering instability induced in [Budin & Szostak (2011)] when oleo-lipids were added to the bulk of the spherical bilayer suspension. The fingering instability corresponds to a backward heat flow in the curvature. The resulting singularity is associated to the development of the pore type growth form the bilayer surface. Moreover, in [Doelman et al (submitted)] the condition $\gamma_1 > \gamma_b^*$ was identified as the point of bifurcation to linear instability of the meander eigenvalues associated to spherical bilayers. For $\gamma_1 < \gamma_b^*$ the curvature driven flow is locally well-posed but is subject to finite-time blow-up due to the cubic driving force, H_0^3. This is the familiar finite-type extinction of droplets under curvature driven flow. However, for the quenched flow (5.4) the relaxation of γ_1 to its equilibrium value precludes the blow-up if the initial curvatures are not too large.

A similar reduction can be performed for co-dimension two pore structures, parametrized by the one-dimensional immersion Γ_p. The result is a similar quenched curvature driven flow for the vector valued normal velocity $\vec{V}_p = -(\frac{\partial z_1}{\partial_{t_1}}, \frac{\partial z_2}{\partial_{t_1}})^T$,

$$\begin{aligned} \vec{V}_p &= \nu_p(\gamma_1 - \gamma_p^*)\vec{\kappa}(s), \\ \frac{d\gamma_1}{dt_1} &= -\varepsilon m_p(\gamma_1 - \gamma_p^*) \int_{\Gamma_p} |\vec{\kappa}|^2 \, ds, \end{aligned} \tag{5.6}$$

where $\nu_p := \frac{m_p}{\pi \int_0^\infty (\phi_p')^2 R\, dR} > 0$, $\vec{\kappa}$ is the vector curvature of Γ_p, $m_p := 2\pi \int_0^\infty (\phi_p - b_-) R\, dR$ is the mass of amphiphilic material per unit length of pore structure and the equilibrium value

$$\gamma_p^* := -\frac{\eta_1}{\alpha_-^2} \frac{\int_0^\infty (\phi_p')^2 R\, dR}{\int_0^\infty (\phi_p - b_-)^2 R\, dR}, \tag{5.7}$$

is again independent of Γ_p. Most intriguingly, initial data corresponding to spatially separated pores and bilayers yields a competitive evolution that can be understood as a fight for surfactant, mediated through the common value of the bulk amphiphilic density γ_1, whose evolution is determined to impose the conservation of total mass,

$$\begin{aligned} V_n &= \nu_b(\gamma_1 - \gamma_b^*)H \\ \vec{V}_p &= \nu_p(\gamma_1 - \gamma_p^*)\vec{\kappa} \\ \frac{d\gamma_1}{dt_1} &= -\nu_b m_b(\gamma_1 - \gamma_b) \int_{\Gamma_b} H_0^2 dS - \varepsilon \nu_p m_p (\gamma_1 - \gamma_p^*) \int_{\Gamma_p} |\vec{\kappa}|^2 \, ds, \end{aligned} \tag{5.8}$$

The competitive evolution of the bilayers and pores couples through curvature-weighted surface area. However, the two morphologies seek differing equilibria values, which typically satisfy $\gamma_b^* > \gamma_p^*$, making coexistence of bilayers and pores impossible under the strong functionalization, unless one of the structures is flat, since zero curvature interfaces are at equilibrium independent of bulk value of amphiphile. For curved interfaces, the range $\gamma_1 \in [\gamma_p^*, \gamma_b^*]$ is invariant under the flow, and once γ_1 enters this range the bilayers will shrink, while the pore morphologies will grow. Moreover, if the pearling threshold P_* lies within the invariant range $[\gamma_p^*, \gamma_b^*]$ then the value of γ_1 may transiently decrease through the pearling threshold for bilayers, (4.21), causing the bilayers to pearl as they shrink. Various realizations of this transient interaction are depicted in Figure 5.1, for double wells W with increasing well tilt.

6 Conclusion

The Functionalized Cahn-Hilliard free energy provides a compact description of the energy landscape driving morphological selection in amphiphilic mixtures, such as lipid bilayers. We have shown that the strength of the interactions of the hydrophilic units with the solvent phase, parameterized by $\eta_1 > 0$, the packing entropy of the hydrophobic tails, parameterized by η_2, and the pressure jump between amphiphilic and hydrophobic phases, characterized by the difference in self energies, $W(b_\pm)$ of the amphiphilic and bulk phases, can trigger a range of bifurcations. Specifically the fingering and pearling instabilities observed experimentally in [Budin & Szostak (2011)] and [Zhu et al (2012)] by adjusting the bulk values of lipids and the charge density of the lipids, respectively, can be induced in the FCH framework by varying the corresponding control parameters. There are however many avenues to explore, for example the pearling bifurcation induces a periodic dimpling of a bilayer surface which can lead to perforation. Within the biological context of cell membranes, it is of particular interest to understand the energy required to open a single hole. Can a local adjustment of parameter values, such as a spatial variation in η_1, induce the opening of isolated holes in the membrane?

Acknowledgements

The second author acknowledges the support of the DMS of the National Science Foundation through grant 1109127. Both authors thank Andrew Christlieb and Jaylan Jones for the computations which resulted in the images presented in Figures 4.3 and 5.1.

References

[Andreussi et al (2012)] O. Andreussi, I. Dabo, and N. Marzari, Revised self-consistent continuum solvation in electronic-structure calculations, *J. of Chemical Physics*, **136** 064102 (2012).

[Budin & Szostak (2011)] I. Budin and J. Szostak, Physical effects underlying the transition from primitive to modern cell membranes, *Proc. National Academy Science*, **108** 5249-5254 (2011).

[Cahn & Hilliard (1958)] J.W. Cahn and J.E. Hilliard, Free energy of a nonuniform system. I. Interfacial free energy, *J. Chem. Phys.*, **28** 258-267 (1958).

[Charleux et al (2012)] B. Charleux, G. Delaittre, J. Rieger, and F. D'Agosto, Polymerization-Induced Self-Assembly: from soluble macromolecules to block copolymer nano-objects in one step, *Macromolecules*, **45** 6753-6765 (2012).

[Chavel I.(1984)] I. Chavel, *Eigenvalues in Riemannian Geometry*, London: Academic Press, (1984).

[Dai & Promislow (2013)] S. Dai and K. Promislow, Geometric Evolution of Bilayers under the Functionalized Cahn-Hilliard equation, *Proc. Roy. Soc. London, Series A*, **469** (2013).

[Dai & Promislow (submitted)] S. Dai and K. Promislow, Competitive Geometric Evolution of Amphiphilic Interfaces, submitted.

[Doelman et al (submitted)] A. Doelman, G. Hayrapetyan, K. Promislow, and B Wetton, Meander and pearling of single-curvature bilayer interfaces in the Functionalized Cahn Hilliard equation, submitted.

[Discher & Eisenberg (2002)] D. Discher & A. Eisenberg, Polymer Vesicles, *Science*, **297** 967-973 (2002).

[Hayrapetyan & Promislow (2014)] G. Hayrapetyan and K. Promislow, Spectra of Functionalized Operators arising from hypersurfaces, to appear in *ZAMP* (2014).

[Gavish et al (2011)] N. Gavish, G. Hayrapetyan, K. Promislow and L. Yang, Curvature driven flow of bi-layer interfaces, *Physica D*, **240** 675-693 (2011).

[Gavish et al (2012)] N. Gavish, J. Jones, Z. Xu, A. Christlieb and K. Promislow, Variational Models of Network Formation and Ion Transport: Applications to Peruorosulfonate Ionomer Membranes, *Polymers*, **4** 630-655 (2012).

[Gomez et al (2005)] E. Gomez, T. Rappl, V. Agarwal, A. Bose, M. Schmutz, C. Marques, and N. Balsara, Platelet self-assembly of an amphiphilic A-B-C-A tetrablock copolymer in pure water, *Macromolecules*, **38** 3567-3570 (2005).

[Gompper & Schick (1990)] G. Gompper and M. Schick, Correlation between structural and interfacial properties of amphiphilic systems, *Phys. Rev. Lett.*, **65** 1116-1119 (1990).

[Jain & Bates (2004)] S. Jain and F. Bates, Consequences of nonergodicity in aqueuos binary PEO-PB micellar dispersions, *Macromolecules*, **37** 1511-1523 (2004).

[Kapitula and Promislow (2013)] T. Kapitula and K. Promislow, *Spectral and dynamical stability of nonlinear waves*, Springer, N.Y. (2013).

[Kraitzman (thesis)] Noa Kraitzman, Bifurcation and Competitive Evolution of Network morphologies in the strong Functionalized Cahn-Hilliard equation. PhD thesis (2015).

[Matyjaszewski (2012)] K. Matyjaszewski, Atom Transfer Radical Polymerization (ATRP): Current Status and Future Perspectives *Macromolecules*, **45** 4015-4039 (2012).

[Pego (1989)] R.L. Pego, Front migration in the nonlinear Cahn-Hilliard equation, *Proc. R. Soc. Lond. Ser. A*, **422** 261-278 (1989).

[Promislow & Zhang (2013)] K. Promislow and H. Zhang, Critical points of functionalized Lagranagians, *Disc. Cont. Dynamical Systems, A*, **33** 1-16 (2013).

[Ratcliffe et al (2013)] L. Ratcliffe, A. Ryan, and S. Armes, From a Water-Immiscible Monomer to Block Copolymer Nano-Objects via a One-Pot RAFT Aqueous Dispersion Polymerization Formulation, *Macromolecules*, **46** 769-777 (2013).

[Roger & Schatzle (2006)] M. Röger, R. and Schätzle, On a modified conjecture of De Giorgi, *Math. Z.*, **254** 675-714 (2006).

[Scherlis et al (2006)] D.A. Scherlis, J.L. Fattebert, F. Gygi, M. Cococcioni, and N. Marzari, A unified electrostatic and cavitation model for first-principles molecular dynamics in solution, *J. Chem. Phys.*, **124** 074103 (2006).

[Teubner & Strey (1987)] M. Teubner and R. Strey, Origin of scattering peaks in microemulsions, *J. Chem. Phys.*, bf 87 3195-3200 (1987).

[Zare et al (2012)] P. Zare, A. Stojanovic, F. Herbst, J. Akbarzadeh, H. Peterlik, and W.H. Binder, Hierarchically Nanostructured Polyisobutylene-Based Ionic Liquids, *Macromolecules*, **45** 2074-2084 (2012).

[Zhu & Hayward (2012)] J. Zhu and R.C. Hayward, Interfacial tension of evaporating emulsion droplets containing amphiphilic block copolymers: Effects of solvent and polymer composition, *J. Colloid and Interfacial Science*, **365** 275-279 (2012).

[Zhu et al (2009)] J. Zhu, N. Ferrer, and R.C. Hayward, Tuning the assembly of amphiphilic block copolymers through instabilities of solvent/water interfaces in the presence of aqueous surfactants, *Soft Matter*, **5** 2471-2478 (2009).

[Zhu et al (2012)] T.F. Zhu, K. Adamala, N. Zhang, and J.W. Szostak, Photochemically driven redox chemistry induces protocell membrane pearling and division, *Proceedings National Academy Science*, **109** 9828-9832 (2012).

[Zhulina & Borisov (2012)] E.B. Zhulina and O.V. Borisov, Theory of Block Polymer Micelles: Recent Advances and Current Challenges, *Macromolecules*, **45** 4429-4440 (2012).